2023-11

Experimental study of interactions between focused waves and a point absorber wave energy converter

Zhu, Guixun

10.1016/j.oceaneng.2023.115815
Ocean Engineering
Elsevier BV

Ocean Engineering 287 (2023) 115815

Contents lists available at ScienceDirect

Ocean Engineering

journal homepage: www.elsevier.com/locate/oceaneng

Experimental study of interactions between focused waves and a point absorber wave energy converter

Guixun Zhu [a,b,*], Zahra Shahroozi [c], Siming Zheng [a], Malin Göteman [c,d], Jens Engström [c], Deborah Greaves [a]

[a] School of Engineering, Computing and Mathematics, University of Plymouth, Drake Circus, Plymouth PL4 8AA, UK
[b] Department of Mechanical Engineering, National University of Singapore, Singapore 119260, Singapore
[c] Department of Electrical Engineering, Uppsala University, Ångströmlaboratoriet, Lägerhyddsvägen 1, 752 37 Uppsala, Sweden
[d] Centre of Natural Hazards and Disaster Science (CNDS), Villavägen 16, 752 36 Uppsala, Sweden

ARTICLE INFO

Keywords:
Wave energy converter
Point absorber
Focused wave
Wave-structure
Mooring force

ABSTRACT

Predicting the response of point absorber wave energy converters (WECs) in extreme sea states is crucial for assessing their survivability. However, data are scarce and hydrodynamic understanding is limited. In order to simulate extreme wave conditions, laboratory-scale focused waves based on NewWave theory have been utilized. To investigate the interactions between focused waves and a point absorber WEC, a wave basin experiment has been conducted. Various parameters, including focusing amplitude and peak frequency have been examined across three different damping conditions. The motion response of the point absorber WEC and the corresponding mooring force have been measured over time. The experimental findings reveal that both the focused wave parameters and the damping values have a significant influence on the motion response and mooring force. It is shown that an increase in the focusing amplitude leads to a more intense motion response, while the mooring force is relatively insensitive to the focused amplitude/peak frequency when the end-stop spring is not compressed. The force in the connection line is maximized when the upper end-stop spring is compressed. As the peak frequency increases, the heave and surge responses decrease, whereas the maximum mooring force increases with peak frequency for a locked power take-off (PTO) system. Finally, the results indicate that optimizing the design of the power take-off system, including selecting appropriate damping values and stroke lengths for the translator, can significantly reduce the mooring load for extreme wave conditions.

1. Introduction

Climate change and escalating energy demand worldwide have highlighted the urgent need for clean, sustainable, and renewable energy, which has become a paramount focus of global development. Despite the considerable attention that wind and solar energy have garnered for their efficient utilization of natural resources, there has been a recent surge in the exploration of wave and tidal energy conversion technologies. Wave energy represents an abundant and eco-friendly resource that offers multiple benefits, including predictable and consistent topology and high energy density (Zhang et al., 2021), rendering it an appealing option for coastal countries (Lehmann et al., 2017; Jin and Greaves, 2021).

To this end, numerous wave energy converter (WEC) designs have been proposed, mainly including oscillating water columns (Falcão and Henriques, 2016; Ning et al., 2019; Zheng et al., 2019; Zhu et al., 2023), oscillating wave surge converters (Brito et al., 2020b,a), overtopping devices (Margheritini et al., 2009; Contestabile et al., 2020), and point absorbers (Al Shami et al., 2018; Guo et al., 2022; Li and Liu, 2022; Soleimani et al., 2023). Among these, point absorbers are considered one of the most straightforward WECs, with a characteristic length typically smaller than the wavelength at the peak wave frequency (Budal and Falnes, 1975; Faizal et al., 2014). Its small dimensions allow the device to be wave-direction independent and capable of absorbing power from all the wave directions, which can be highly varied during the life of the device. Additionally, many point absorber technologies have the advantage of easy fabrication and installation (Drew et al., 2009; Cretel et al., 2011).

The point absorbers utilized in wave energy conversion systems must be designed to withstand the largest waves encountered during storms of magnitude equal to that of their intended operating

* Corresponding author at: School of Engineering, Computing and Mathematics, University of Plymouth, Drake Circus, Plymouth PL4 8AA, UK.
E-mail address: grant_zhugx@outlook.com (G. Zhu).

https://doi.org/10.1016/j.oceaneng.2023.115815
Received 6 June 2023; Received in revised form 3 August 2023; Accepted 7 September 2023
Available online 18 September 2023

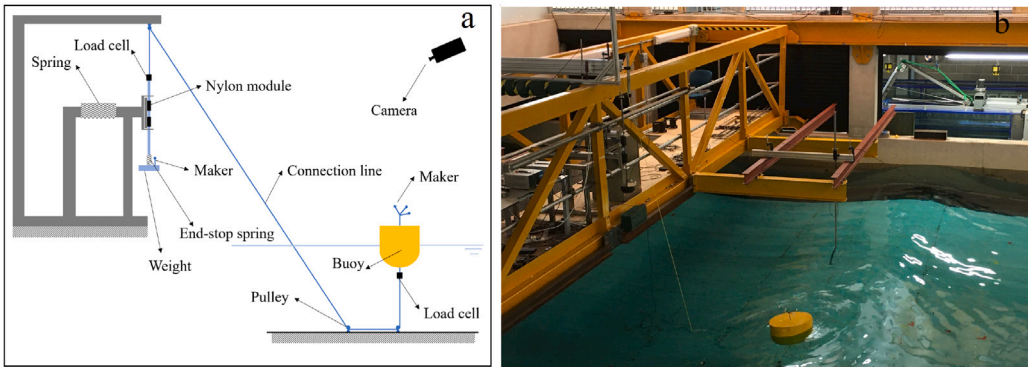

Fig. 1. The sketch of the wave tank experiment (a) and physical study carried out at the University of Plymouth (b).

conditions (Hann et al., 2015). Exploring the behaviour of point absorbers under extreme sea states is essential for gaining insight into their performance in challenging environments, thereby aiding in the development of more robust and reliable systems. Adverse weather conditions, such as those induced by storms or hurricanes, may expose the point absorbers to substantial mechanical and hydrodynamic loads that may affect their structural integrity and functional efficacy. However, due to the inherent uncertainties associated with predicting the magnitude and characteristics of these loads, conservative assumptions are often made in the design process (Giannini et al., 2022; Garcia-Teruel and Forehand, 2022). The design standards need to be tailored for the wave energy sector since there are large uncertainties related to the prediction of wave loads on WECs. The devices are small and often with dynamical behaviour, designed to be in resonance with the waves, therefore, the established knowledge from the traditional offshore industry cannot be readily translated to WEC design (Katsidoniotaki et al., 2021). The extreme wave impact on WECs, survivability, and failure risk mitigation are issues that need to be addressed. Experimental and numerical methods are both used to simulate a device's response to extreme waves (Hann et al., 2015). Although numerical simulations have advanced significantly, accurately capturing non-linear effects without over- or underestimating them remains a daunting task. Experimental wave tank tests can be valuable tools for gaining a deeper understanding of the impact of the wave on non-linear phenomena and for validating numerical simulations.

Design procedures for the operational envelope must be complemented by a level of design that accounts for extreme wave spectral parameters and survivability boundaries in experiments (Clauss, 2010). Extreme waves are sporadic events within a random sea state, making their prediction and reproduction difficult. However, a "design-wave" can be constructed to examine the maximum surface elevations and loads due to extreme events in a reproducible, deterministic way (Ransley et al., 2017). In offshore engineering, the NewWave design-wave is the standard for modelling extreme wave interactions with offshore structures (Lindgren, 1970; Tromans et al., 1991; Jonathan and Taylor, 1997; Taylor and Williams, 2004). NewWave theory is often used to generate an extreme wave time series, which models the statistically most probable surface elevation shape associated with the occurrence of an extreme wave crest (Cassidy et al., 2001; Hann et al., 2018). Compared to relying on randomly occurring extreme events in an irregular time series of the sea state, NewWave theory generates an extreme event within a relatively short time series. This feature allows all important wave-structure interactions to occur before significant influence from wave reflections from basin walls occur and makes NewWave focused wave groups ideal to be considered in the wave tank experiments for validating computationally expensive CFD models.

NewWave theory has been widely adopted to investigate extreme wave interactions in various applications. In offshore environments, fixed cylinders have been the subject of experimental and numerical assessments to evaluate the impact of extreme waves using NewWave theory (Walker and Taylor, 2005; Bai and Taylor, 2007; Zang et al., 2010; Bihs et al., 2017; Chen et al., 2022b). NewWave theory has been applied to investigate the impact of extreme waves in the coastal environment (Borthwick et al., 2006; Whittaker et al., 2017; Judge et al., 2019). Additionally, NewWave theory is also used to detect the ultimate response of floating structures, including structural motion response and mooring load, both in numerical (Westphalen et al., 2012; Zhao et al., 2014; Chen et al., 2022a, 2023) and experimental (Göteman et al., 2015; Ransley et al., 2020) work. Moreover, the NewWave theory has been applied to study point absorber WECs. Rafiee and Fiévez (2015) modelled a point absorber under moderate and extreme conditions. The OpenFOAM simulation of focused waves resulted in an underestimation of extreme values. Ransley et al. (2017) verified the accuracy of the numerical model to predict the survivability of the point absorber WECs by simulating the interaction between the focusing wave and the buoy. Hann et al. (2018) measured a moored floating body's interaction with extreme waves, indicating a negligible effect on peak mooring loads but significant differences in motion. Katsidoniotaki et al. (2021) evaluated the survivability of a point-absorbing WEC in the North Sea using OpenFOAM simulations, showing high loads induced by steep and high waves with significant nonlinear phenomena. Shahroozi et al. (2022) found that irregular waves, rather than focused waves, are the most conservative choice in assessing the extreme waves as they show the highest peak force. These studies and other (Jin et al., 2018; Brown et al., 2020) found that in addition to considering the most extreme wave likely to occur, it is also important to take into account the motion response of the structure when encountering the wave.

This paper investigates the dynamics of a point-absorbing WEC in focused wave groups. Inspired by Shahroozi et al. (2022), a similar buoy and power take-off (PTO) system have been used in this work. The aim of this research is to investigate the effects of focused waves on point absorbers, and evaluate the influence of different PTO damping on the motion response and mooring force. In order to achieve this goal, the geometric parameters of the device were held constant, and the study focused on measuring the dynamic responses of the system under various wave conditions. Section 2 describes the experimental setup. Results and discussions are described in Section 3. Finally, conclusions are drawn in Section 4.

2. Methodology and experimental setup

In this section, the wave tank experiment conducted in the Ocean and Coastal Engineering Laboratory of Plymouth University is described. The experimental setup is depicted in Fig. 1. Focused wave theory is introduced in Section 2.1. The point absorber WEC is described in Section 2.2. The measuring equipment and its settings are described in Section 2.3.

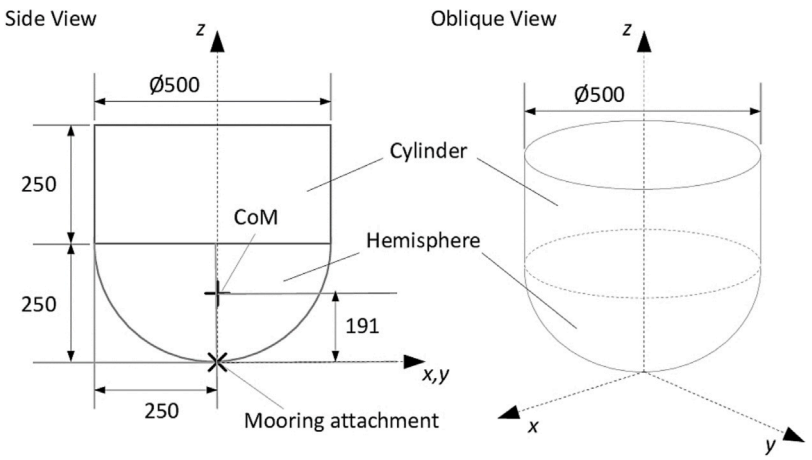

Fig. 2. Sketch of the buoy (in millimetre) (Ransley et al., 2020).

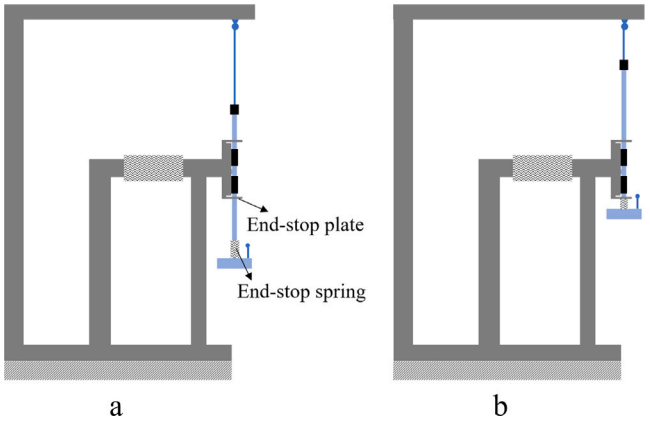

Fig. 3. The sketch of the PTO system at the initial position (a) and the translator moves while the end-stop spring compresses (b).

2.1. NewWave focused wave group

A focused wave group is composed of multiple regular waves, each with a specific frequency and amplitude, whose phases are adjusted such that their crests coincide at a predetermined position and time. We utilized a focused wave group based on the NewWave concept (Tromans et al., 1991), which is compact and generates only two or three waves resulting in wave crest when the input is derived from a Pierson–Moskowitz (PM) spectrum. The choice of the spectrum is essential, as the amplitude spectrum of the compact wave group must correspond to the energy spectrum of the presumed random sea, from which the extreme wave packet is obtained (Hunt-Raby et al., 2011).

The NewWave focused wave group, based on a probabilistic analysis of the shape of a maximum in a linear, Gaussian process, describes the most probable shape of a large wave in a given sea state. Lindgren (1970) showed that the shape of a large event (wave) comprises both deterministic and random components, with the deterministic component dominating for events that are relatively large to the underlying process (sea state). The theory is applied by decomposing a finite number of first-order wave components from a sea spectrum using the fast Fourier transform (FFT) method by considering a design focal time and focal distance (Westphalen et al., 2009). The focused wave theory formula is as follows:

$$\eta(x,t) = \sum^{N} a_n \cos(k_n(x - x_f) - (t - t_f) + \epsilon_n). \tag{1}$$

where a_n is the wave amplitude, k_n is the component wave number obtained using the linear dispersion relation and ϵ_n is the initial component phase. The design focal distance x_f is the desired distance from the wavemaker paddles, and the design focal time t_f is the time required for the wave to travel this distance. For crest-focused waves $\epsilon_n = 0$, with the origins of both the distance and time scales being fixed at the focused wave event. The wave component amplitudes necessary to generate NewWave, a particular form of focused wave group, are given by Hunt-Raby et al. (2011)

$$a_n = \frac{A_N S_n(\omega)\delta\omega_n}{m_0} = \frac{A_N S_n(\omega)\delta\omega_n}{\sum_n S_n(\omega)\delta\omega_n}, \tag{2}$$

where $S_n(\omega)$ is the discretized energy spectrum, $\delta\omega_n$ the frequency increment and $A_N = [2m_0 \ln(N)]^{1/2}$ in which m_0 is the zeroth moment of the energy spectrum. Further, N denotes the use of NewWave as a model for the largest in N waves drawn from the assumed underlying random sea state, assuming Rayleigh statistics for wave height. Moreover, $N = 1000$ is considered in this work. The Pierson–Moskowitz (PM) spectrum was used to produce the focused waves in this work, which exhibits a less prominent peak than the JONSWAP spectrum (Ning and Ding, 2022). The theoretical wave representation is equated to physical wave generation in a wave tank by taking the position of the wavemaker paddle x as zero. Furthermore, the focused wave technique was implemented by modifying Eq. (1) to create a time history of paddle stroke displacements. Throughout this study, 24 individually controlled hinged flap absorbing paddles were used to generate focused waves in the COAST laboratory Ocean Basin, University of Plymouth.

2.2. Point absorber wave energy converter

The point absorber WEC comprises two parts, the floating body (buoy) and the PTO system. The two bodies are connected via a rope. The floating body moves with the waves and moves the PTO translator by the connected rope.

A 1:20 scaled, hemispherical-bottomed, cylindrical buoy with a stiff Dyneema connection line has been used. The scale was determined by comparing the buoy size with Shahroozi et al. (2022)'s experiment. The buoy is was designed and used for numerical modelling and experimental studies as reported by Hann et al. (2015, 2018), Ransley et al. (2020) and Ransley et al. (2021). The buoy is 0.5 m in diameter with a 0.25 m tall cylindrical section above its hemispherical bottom (Fig. 2). It has ballast weight secured within the hemispherical part. This buoy is manufactured from 2 mm thick mild steel. Therefore, a ballast weight is placed inside the hemisphere to change the weight distribution to ensure that the form of the buoy is always hemispherical downwards (in general). At the same time, ballast weight is considered

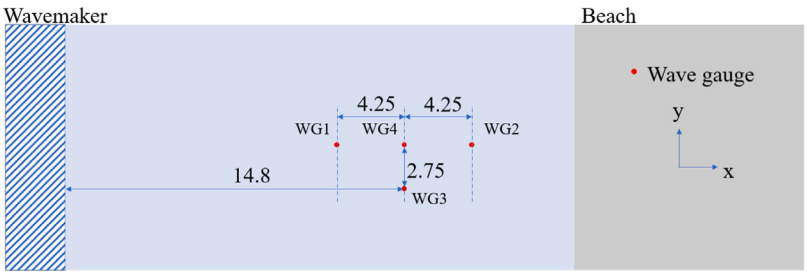

Fig. 4. Wave tank dimensions (in metres) and wave gauges positions, where the buoy is situated in the location of wave gauge 4.

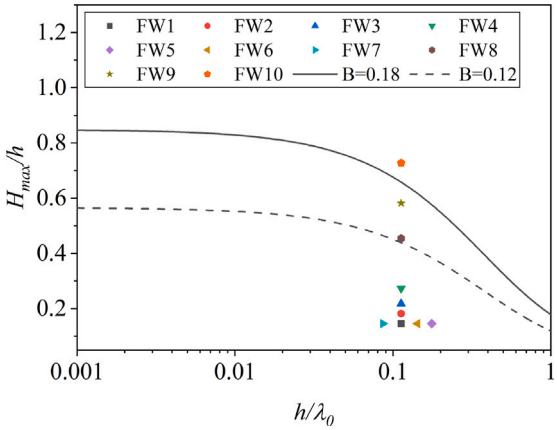

Fig. 5. Evaluation of focused wave breaking index.

Table 1
Experimental cases.

Case	A_f (m)	f_p (Hz)	K_pA_f	X_f (m)
FW1	0.08	0.40	0.0686	14.8
FW2	0.10	0.40	0.0857	14.8
FW3	0.12	0.40	0.1029	14.8
FW4	0.15	0.40	0.1286	14.8
FW5	0.12	0.50	0.1406	14.8
FW6	0.12	0.45	0.1215	14.8
FW7	0.12	0.35	0.0883	14.8
FW8	0.25	0.40	0.2143	14.8
FW9	0.32	0.40	0.2743	14.8
FW10	0.40	0.40	0.3429	14.8

to satisfy scale effects. The total mass is 43.2 kg centred 0.191 m above the bottom mooring point. The moment of inertia of the buoy is $(I_{xx} \times I_{yy} \times I_{zz}) = (1.62 \times 1.62 \times 1.143)$ kg m^2. Restrained only by a single-point mooring, which attaches at the bottom of the buoy where the symmetry axis intersects the surface of the hemisphere, the structure in this case is able to move in all six degrees of freedom. The connection line between the buoy and the PTO not only transmits the tension caused by the movement of the buoy but also has a mooring effect on the buoy.

A linear friction-damping PTO is designed and used, see Fig. 1. This PTO consists of a rod connected to two linear guides for providing a smooth and robust movement with minimal vibration, two spring-Nylon modules for applying a constant sliding friction damping force, and an end-stop spring. A pretension spring with a coefficient of 6.48 N/mm is used. The pressure applied to the nylon modules is changed by the length of the pretension spring. This results in a change in the friction of the bearing, which in turn affects the damping of the PTO system. In total, three PTO damping configurations are tested that are d_0, d_1, and d_∞ for which the first two correspond to the sliding friction damping force of 0 N and 27 N, and the third one represents the infinite damping coefficient where the PTO is locked. For damping configurations 0 (d_0), the spring-Nylon module is free to move. Thus, the friction applied to the bearing is zero. A rod and attached weights equivalent to the mass of the PTO are considered at this moment. Note that the damping configurations discussed throughout the paper refer to the PTO damping cases. The PTO mass, which includes the translator mass and all the attached equipment is 6.0 kg.

In this setup, the translator motion is constrained only by an upper end-stop, as shown in Fig. 3. The purpose of the end-stop spring in the full-scale system is to prevent the moving parts of the generator from hitting the hull (Katsidoniotaki et al., 2021; Shahroozi et al., 2022). The end-stop spring with a coefficient of 13.73 N/mm is used whose uncompressed and compressed lengths are 50.8 mm and 21 mm, respectively. The stroke length of 330 mm is considered. The translator can move up to 165 mm before fully compressing the upper end-stop spring. Moreover, there is no lower end-stop in the system.

2.3. Measurement

To measure the position of the translator and the buoy, a Qualisys system equipped with four cameras and a sampling rate of 128 Hz is used to track the buoy and the weight at the end of the PTO system. The force data is collected by two load cells, one connected between the line and the PTO translator and the other at the connection between the mooring and buoy. The measurement systems, including load cells, Qualisys system, and wave gauges, are calibrated. In this paper, we present results for the load cell connected to the PTO translator. The surface elevation is measured using four wave gauges placed at different distances from the buoy: one in front of it, one at the back, and two in close proximity to it. The buoy is positioned in the middle of the tank, 14.8 m away from the wavemaker. Fig. 4 illustrates the wave gauge arrangement during wave calibration in an empty wave tank before the buoy is positioned at the location of WG4.

2.4. Case conditions

All the focused wave parameters used in the experiment are listed in Table 1. The wave direction is along the x-axis (Only the heave, surge, and pitch responses are taken into account, owing to the wave's propagation along the x direction). In the experiments, the depth of the water is 1.1 m. The wave amplitude A_f at the focused point was varied from 0.08 m to 0.4 m. As wave conditions change, broken focused waves may occur. Identifying whether the waves in a particular sea state break may be pursued using breaking criteria. Goda (2010) presented a formula for the breaking index for a range of mild and a zero beach slope, using the following equation:

$$\frac{H_{max}}{h} = \frac{B}{h/\lambda_0}\left(1 - exp\left[-1.5\pi\frac{h}{\lambda_0}\right](1 + 11s^{4/3})\right), \quad (3)$$

where H_{max} is breaking wave height, h is the water depth, and s is the beach slope. For this experiment, it is a zero slope condition. B is the proportionality coefficient of the breaking index, which for focused waves is between 0.12 and 0.18. λ_0 is the deep water wavelength of small amplitude waves that is computed based on: $\lambda_0 = (g/2\pi)T_p^2$.

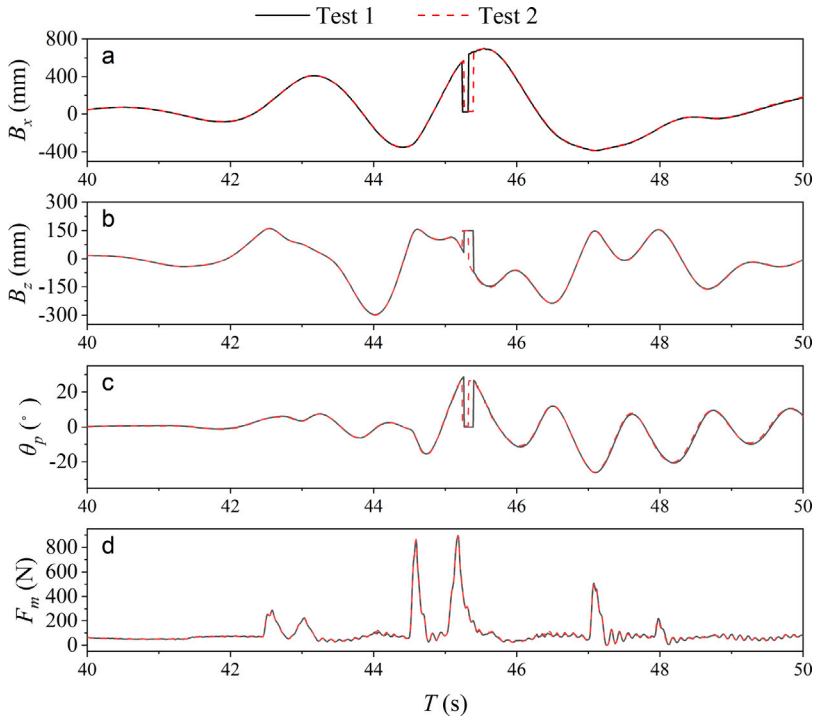

Fig. 6. Time history of the surge (a), heave (b) and pitch (c) responses and mooring forces of the point absorber WEC resulting for case FW10 with the damping values d_0. (B_x, B_z, θ_p and F_m denote the surge, heave, pitch motion and mooring forces relative to the initial values.).

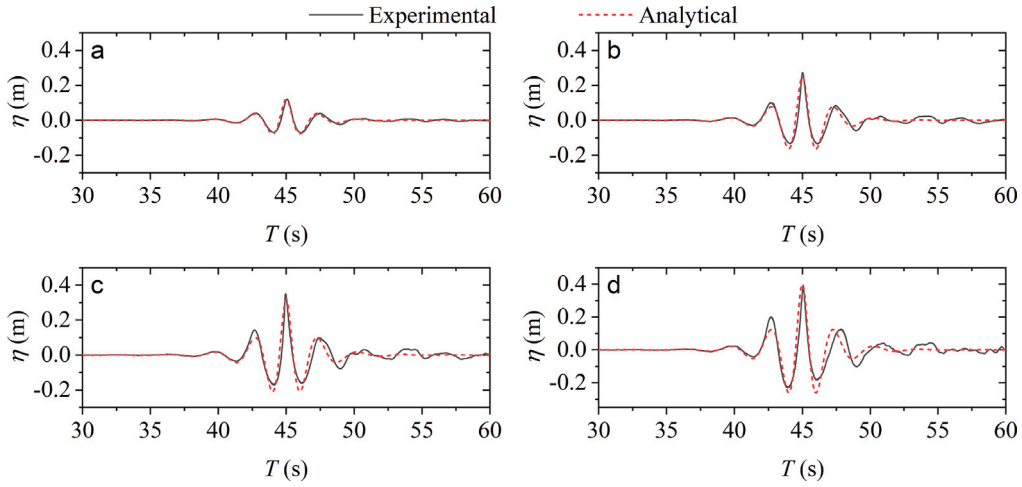

Fig. 7. Comparisons of experimental and analytical surface elevation time-histories for cases FW3 (a), FW8 (b), FW9 (c), and FW10 (d).

Lastly, T_p denotes wave period calculated by the peak frequency. During the wave tank experiment campaign, the wave breaking was mostly observed for FW8, FW9, and FW10 are located on the breaking range as Fig. 5.

In addition, the effect of peak frequency was investigated; the four peak frequencies 0.35 Hz, 0.40 Hz, 0.45 Hz, and 0.50 Hz were considered. Although the focusing amplitude is the same, different peak frequencies lead to different steepness (K_pA_f, where K_p denotes the wavenumber associated with the peak frequency.). The focus time is fixed at 45 s for all cases.

3. Results and discussions

3.1. Repeatability

In this work, each case was tested twice. Fig. 6 shows the motion responses of the buoy and the mooring loads for the FW10 case. From 40 s to 50 s, the surge motions, heave motions, pitch motions and mooring forces of the two experiments are in agreement, except for some minor differences. Therefore, the quality of the experimental data is considered acceptable.

3.2. Wave elevations

In theory, if the focused amplitude is small, the wave nonlinearity is small (Ning et al., 2009). The physically generated wave time series should be identical to the linear theoretical results. To assess the accuracy of an incident wave, Fig. 7(a) compares the time history surface elevation at the focus point of linear and experimental results for case FW3. As expected, the agreement of the two results is good since the incident waves in the experiment are recalibrated. As the focusing amplitude increases, the nonlinearity of the wave increases. In this way, the breaking focused wave occurs for cases FW8, FW9,

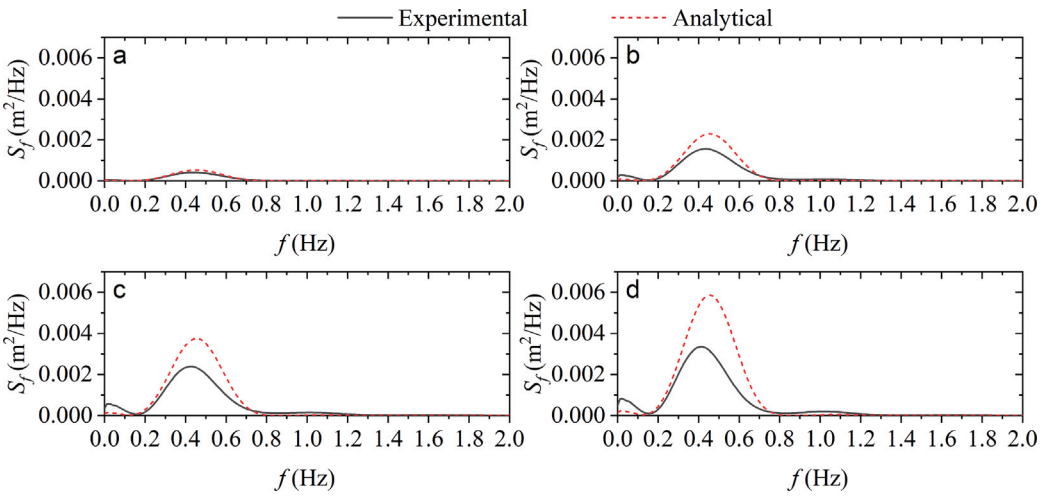

Fig. 8. Comparisons of experimental and analytical spectral density of free surface elevation at the focused position for cases FW3 (a), FW8 (b), FW9 (c), and FW10 (d).

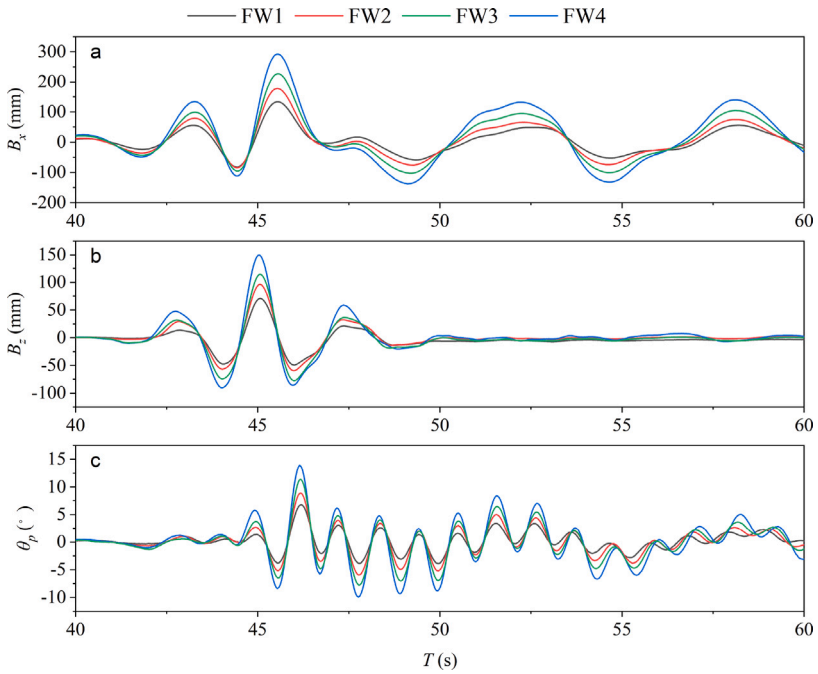

Fig. 9. Time history of the surge (a), heave (b) and pitch (c) response of the point absorber WEC resulting from focused wave groups with different focused amplitude. (B_x, B_z, and θ_p denote the surge, heave and pitch motion relative to the initial position.).

and FW10, which are in the breaking range in Fig. 5. As a result, the evolution of the free surface at the focused position deviates from the theoretical solution for FW8, FW9, and FW10 in Fig. 7(b), (c), and (d). The difference observed at the trough between the analytical and experimental data can be attributed to several factors. These include the steepness of the waves, and the influence of the intermediate water depth, h, that is taken into consideration here. Intermediate waves, where $1/20 < h/L_p < 1/2$ (with L_p being the wavelength based on the peak period), are affected by the presence of the wave tank bed, causing the wave celerity to depend on both the water depth and wavelength (Chakrabarti, 1987).

Further features of the non-linearity of the wave groups are now discussed. Fig. 8 depicts the comparisons of experimental and analytical spectral density S_d of free surface at the focus points, respectively, which are obtained by using FFT of the time-histories of wave elevations in Fig. 7. The close agreement between the experimental and analytical elevations shown as time histories in Fig. 7(a) carries over into the spectral plots. For the cases FW8 (b), FW9 (c), and FW10 (d), as the wave groups are breaking, the energy near peak frequency is much smaller than the analytical value, and the peak frequency is smaller than the analytical value. In addition, the experimental results show that the spectra density is larger than the theoretical value for frequencies less than 0.2 Hz.

3.3. Effect of focused amplitude

In this section, we consider the WEC response in the focused waves. Seven focused wave amplitudes are considered, which are 0.08 m, 0.10 m, 0.12 m, 0.15 m, 0.25 m, 0.32 m, and 0.40 m. These focused waves with various amplitudes correspond to case FW1, FW2, FW3, FW4, FW8, FW9, and FW10, respectively (see Table 1).

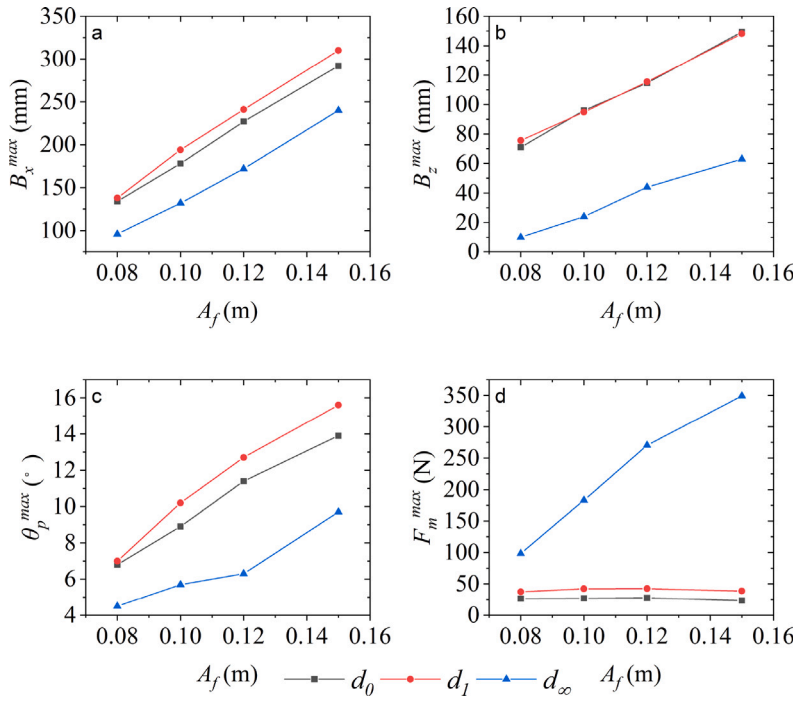

Fig. 10. Maximum surge (a), heave (b), pitch (c), and mooring force (d) response of the point absorber WEC with various damping values vs the focused amplitudes of focused wave groups. B_x^{max}, B_z^{max}, and θ_p^{max} denote the maximum surge, heave and pitch motion relative to the initial position.

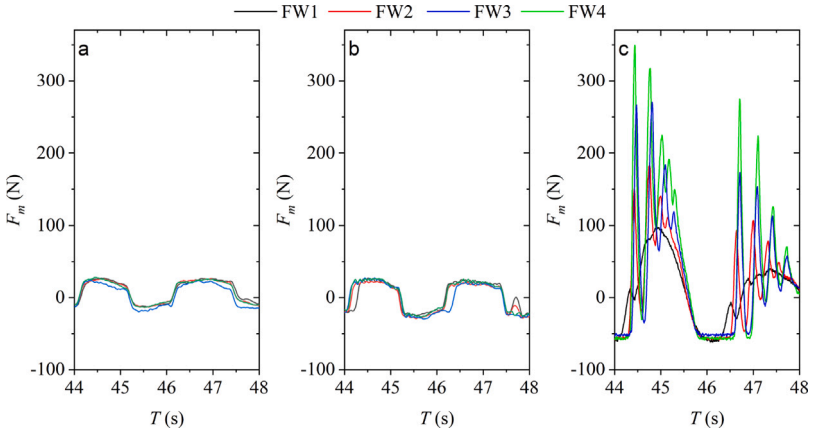

Fig. 11. Time history of the mooring force for different case FW1, FW2, FW3, and FW4 with various damping values d_0 (a), d_1 (b), and d_∞ (c).

To evaluate the effect of the focused wave amplitude on the buoy motion responses, Fig. 9 dshows the heave, surge, and pitch responses of the point-absorbing WEC with the damping values d_∞. With an increase in wave height, the heave, surge, and pitch responses all exhibit heightened magnitudes at the peak. The maximal heave is experienced during the focusing time of the focused wave (around 45 s), whereas the peak values of surge and pitch occur slightly later (around 46 s). The heave rapidly reverts to its initial value post occurrence after 48 s.

To quantitatively compare the influence of the focused amplitude on the motion responses and the mooring load of the buoy, the peak of the motion response and the peak of mooring load are considered. Fig. 10 shows the maximum buoy motion response and mooring forces for various focusing amplitudes and damping cases, at a constant peak frequency 0.4 Hz. The maximum motion and mooring force represent the peak values in its time history. The maximum values of heave, surge, and pitch responses under differing damping values increase with an increase in the peak value. Under various focused amplitudes, the motion response at the infinite damping case d_∞ is smaller than for the other two damping cases. As the PTO damping is designed to dampen the motion, this is an expected result. The heave response is equal for damping case d_0 and damping case d_1, which shows that the chosen damping value d_1 is not sufficiently large to dampen the motion in these large wave conditions. When the focused amplitude is 0.08 m (case FW1), surge and pitch responses are similar. When the damping is d_1, the motion response is the largest, especially the surge and pitch response. It is interesting to see that, while the infinite damping (d_∞) prevents a large motion response of the buoy, it also causes a much larger mooring force as compared to the other two damping cases. The high relative velocity between the buoy and water causes the connection line to tighten when the system is restrained in the locked PTO case. This contributes to the large mooring force, refer to Shahroozi et al. (2022). When damping is d_∞, the maximum mooring force increases with increasing focusing amplitude. The same reason explains why the mooring force at infinite damping increases with the focusing wave amplitude. A more surprising result is that the wave amplitude has very little effect on the maximum mooring force

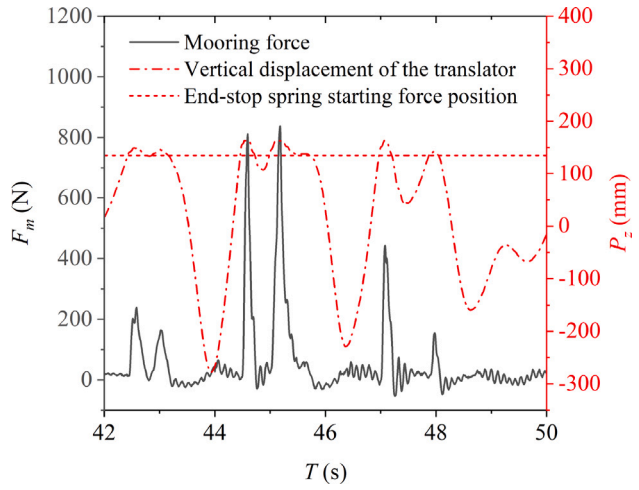

Fig. 12. The mooring force, vertical displacement of the PTO translator, and the end-stop spring starting force position for case FW10 for damping case of d_0. (P_z is vertical displacement.).

for the zero and finite damping values. The lowest mooring force is obtained at zero damping, although the difference between that and the finite damping case is small.

To analyse the mooring force results in more detail, we study the time–history of the mooring force under various damping values and wave amplitudes, shown in Fig. 11. For the zero and finite damping cases, the change in the wave amplitude exerts little influence on the mooring force, which was also known from Fig. 10(d). From Fig. 11 it is clear why - the mooring force in these cases is dominated by the weight of the translator, when the buoy is pulling the translator in the upwards motion. For the infinite damping, on the other hand, the PTO is locked, and the mooring force displays non-linear oscillations of large amplitude, increasing with the wave amplitude. In particular, this occurs when the focusing amplitude is larger than 0.10 m (FW2).

When the focused amplitude continues to increase, the mooring force will also be large where this influence can be seen for d_0 damping case. Fig. 12 shows the time history of the mooring force, as well as the PTO translator displacement. It can be found that sudden increases in mooring forces occur around 42.5 s, 44.5 s, 45.3 s, 47 s, and 48 s. At the corresponding time (corresponding to the sudden increasing mooring forces), the end-stop spring begins to compress. The uncompressed and compressed lengths of the end-stop spring are 50.8 mm and 21 mm, and the end-strop spring starting force position is 135.2 mm. Thus, in the case of large focusing amplitudes, the end-stop spring will reach the top position, causing the connection rope to tighten and experience large mooring forces.

Based on the aforementioned experimental outcomes, a fixed PTO (with infinite damping) is unsuitable for mitigating harsh sea conditions, at least if the key component to be protected from extreme loads is the mooring line. Göteman et al. (2015) found that an increased PTO damping will result in reduced peak loads in the mooring line, which might seem contradictory to the results established here. However, in Shahroozi et al. (2022), both increasing damping values as well as infinite damping were compared, and it was seen that the mooring force reduces with increased damping up to a certain value, but increases again at infinite damping. Our results thereby complement and confirm these earlier established results. Although a fixed PTO can yield a smaller motion response, it may lead to a larger mooring loads than the other damping values. The range of motion of the translator can be set according to sea conditions to avoid large and high frequency changes in mooring force by tightening the mooring rope.

3.4. Effect of peak frequency

For laboratory reproductions of extreme sea states, 50/100-year extreme waves are usually considered. Based on the extreme spectrum, the focused wave technique is used to reproduce the extreme wave under the given sea state. Therefore, the wave spectrum affects the incident focused wave. In this section, four different wave peak frequencies (f_p) of the incident wave spectrum are considered, which are 0.35 Hz, 0.40 Hz, 0.45 Hz, and 0.50 Hz. These focused waves with various peak frequencies correspond to the cases FW7, FW6, FW3, and FW5, respectively.

Fig. 13 presents the time history of the mooring loads measured for different damping values and peak frequencies, at the constant focusing wave amplitude 0.12 m. For d_0 and d_1, the mooring force at the focus time does not change much with the peak frequency. When the focused wave amplitude is 0.12 m, the end-stop spring is uncompressed. Therefore, the mooring forces are mainly affected by the weight of the PTO for d_0 and d_1. Changing the peak frequency has little effect on mooring forces. The peak value of mooring forces at focusing time increases with the increase of peak frequency for the fixed PTO system (d_∞). This trend matches that observed by Hann et al. (2015, 2018). In Fig. 14(d), the maximum mooring forces are shown. The maximum mooring forces under d_∞ are much greater than that under d_0 and d_1. While the maximum mooring forces for damping cases of d_0 and d_1 are less affected by peak frequency.

Fig. 15 shows the spectral density S_D of the mooring force for the different peak frequencies and damping values. The spectral density of damping value d_∞ is much larger than that of damping value d_0 and d_1. This indicates that the mooring force of damping value d_∞ is the largest, which is consistent with the results in Fig. 13. The peak spectral density for the fixed PTO system (d_∞) is more affected (larger increases) by the peak frequency than that of d_0 and d_1. There is also an energy distribution when the frequency is larger than 2.0 Hz. The above analysis shows that when the end-stop spring is not compressed (when the stroke of the translator is long enough), the mooring is little affected by the peak frequency for d_0 and d_1.

To evaluate the influence of the peak frequency on the motion response of the buoy, the time series of the motion responses are compared. Fig. 16 presents the time history of the surge. For d_0, d_1 and d_∞, the peak frequency f_p of the incident wave spectrum shows a similar effect on the surge movement. This result can also be observed from the maximum surge motion in Fig. 14(a). With the decrease of the f_p, the surge responses become lower for all damping conditions. Fig. 17 presents the time history of the heave motion. The maximum heave response with infinite damping (d_∞) occurs with a negative value (i.e., less than the initial position), which is completely opposite to finite damping and zero damping. The peak frequency has the similar impact on heave response at infinite damping. This can also be reflected in the biggest heave response in Fig. 14(b). It is found that the heave responses become lower for all damping conditions with the decrease of the f_p. Fig. 18 presents the time history of the pitch motions. For d_0 and d_1, the peak frequency f_p shows a similar effect on the pitch movement. Whereas the peak frequency has complex effects on the pitch motion for the infinite damping condition (d_∞). Nevertheless, the tendency for the maximum pitch response to increase with the increasing peak frequency holds for all damping conditions. Under different damping conditions, the maximum motion response has the same variation trend with the peak frequency. However, the motion response is minimal for infinite damping.

4. Conclusions

The present study reports the findings of wave tank experiments on a 1:20 scaled model of a point absorber wave energy converter (WEC) with a linear power take-off (PTO) system featuring sliding friction-

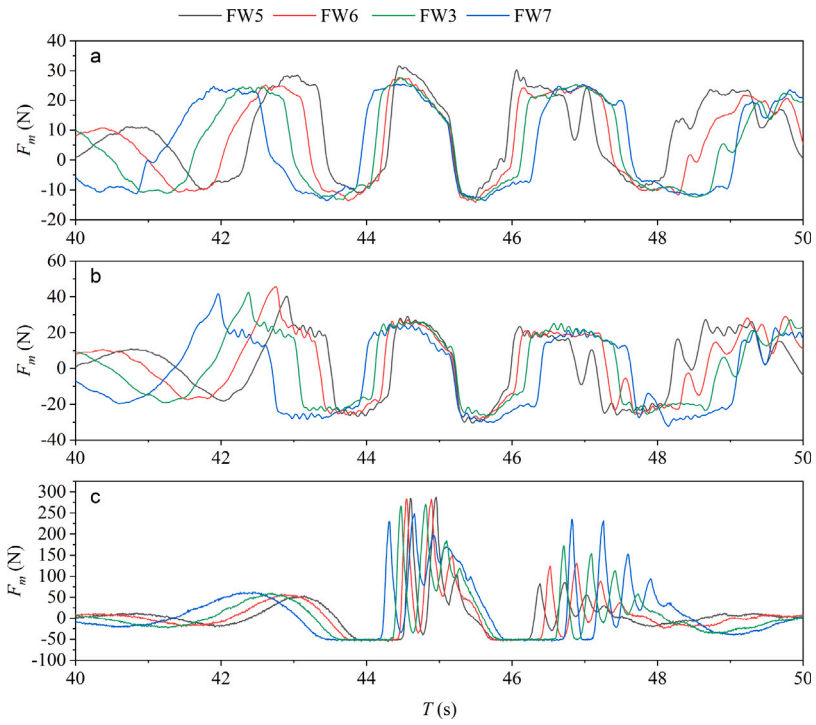

Fig. 13. Time history of the mooring force for different case FW5, FW6, FW3, and FW7 with various damping values d_0 (a), d_1 (b), and d_∞ (c).

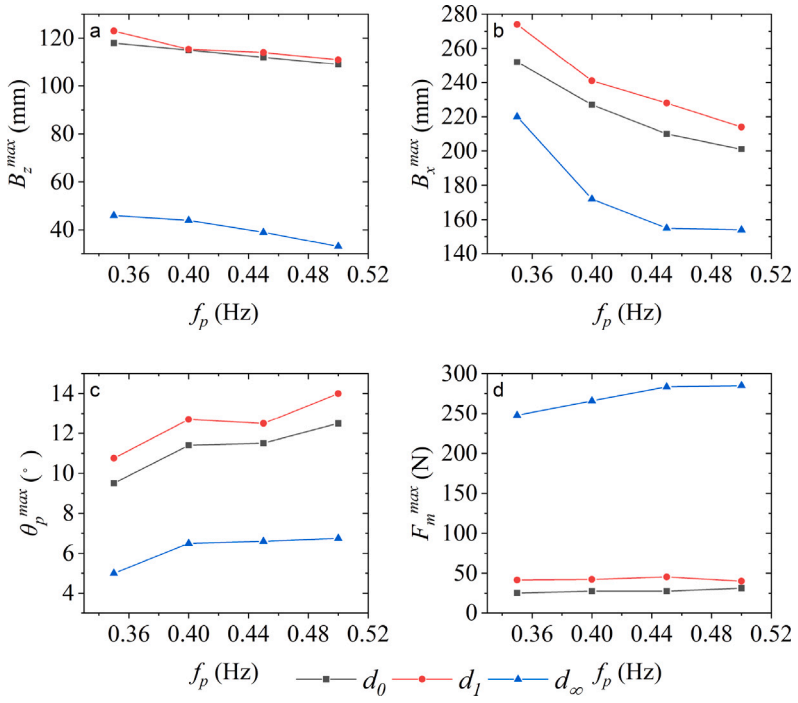

Fig. 14. Maximum heave (a), surge (b), pitch (c) and mooring force (d)response of the point absorber WEC resulting from focused wave groups of increasing steepness with different damping conditions.

damping force, coupled with a cylindrical buoy with an ellipsoidal bottom. The experiments are conducted under twelve different focusing wave states, to examine the response of the WEC and its mooring forces to various focusing amplitudes and peak frequencies. Three different damping forces are considered, namely zero damping (d_0), a finite damping of 27 N (d_1), and an infinite damping (d_∞), resulting in a locked PTO. Finally, the following conclusions can be drawn:

– As the focused wave amplitude increases, the nonlinearity of the wave also increases. The experimental spectral density of the free

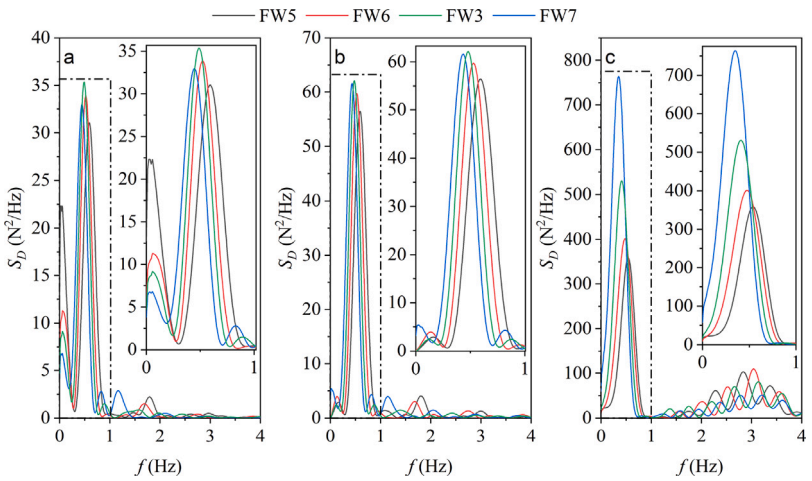

Fig. 15. The spectral density S_D of the mooring force for different case FW3, FW5, FW6, and FW7 with different focused wave steepness for various damping values d_0 (a), d_1 (b), and d_∞ (c).

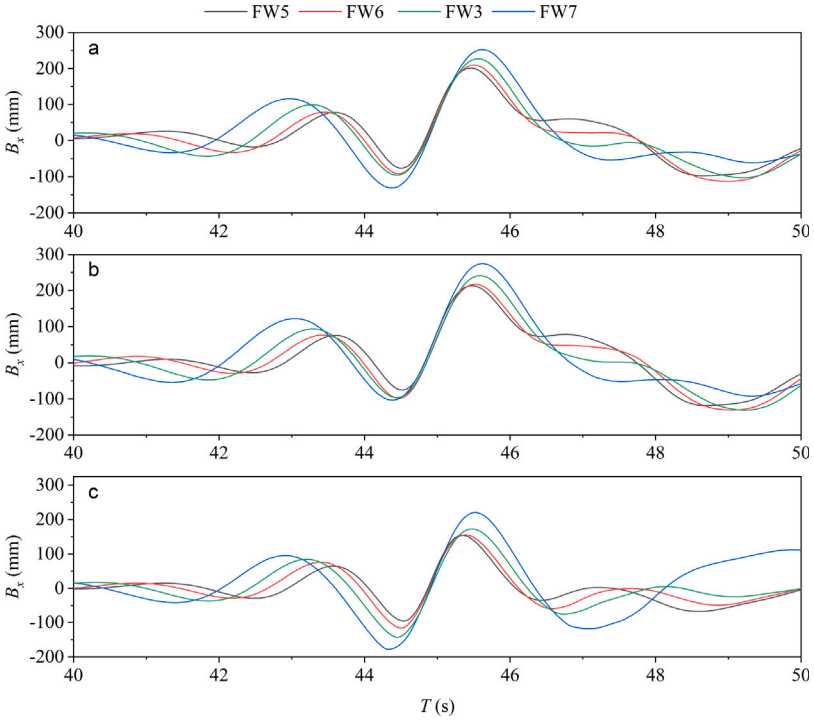

Fig. 16. Time history of the surge motion for different case FW5, FW6, FW3, and FW7 with various damping values d_0 (a), d_1 (b), and d_∞ (c).

surface elevation deviates from the theoretical value for breaking wave cases, with reduction energy near the peak frequency. We demonstrate that non-linear patterns in waves are induced not only by steepness but also by intermediate water depth which results in shallower troughs as shown in Fig. 7.

- As the amplitude of the focused wave amplitude increases while keeping its peak frequency constant, the heave, surge, and pitch responses of the WEC exhibit higher magnitudes. The maximum values of these responses under different damping values increase with an increases in the focused amplitude.
- At a constant wave amplitude, the heave and surge responses reduce with increasing wave peak frequency, while the pitch response increases. The maximum motion response increase with an increase in the peak frequency in the range of wave conditions studied in this work.
- The peak mooring force under d_∞ is significantly greater than under d_0 and d_1, although the motion response under d_∞ is minimal. When the PTO is locked (with infinite damping), the mooring force increases with an increase in the wave amplitude and peak frequency. While peak frequency has little effect on mooring force for the damping values d_0 and d_1 (the PTO translator is not hitting the upper end-stop spring). Large peak loads in the mooring line also occur when the PTO translator hits the upper end-stop spring (for any damping value).

The findings of the wave tank experiments, as presented in this paper, suggest that an infinite damping, corresponding to a locked PTO, is not suitable for mitigating severe sea-state conditions, as it results in larger mooring forces for all cases. For unlocked PTO, sea state has little effect on mooring forces when the end-stop spring is not compressed. However, in the case of zero damping configuration, an extensive load on the structure can lead to an extensive end-stop

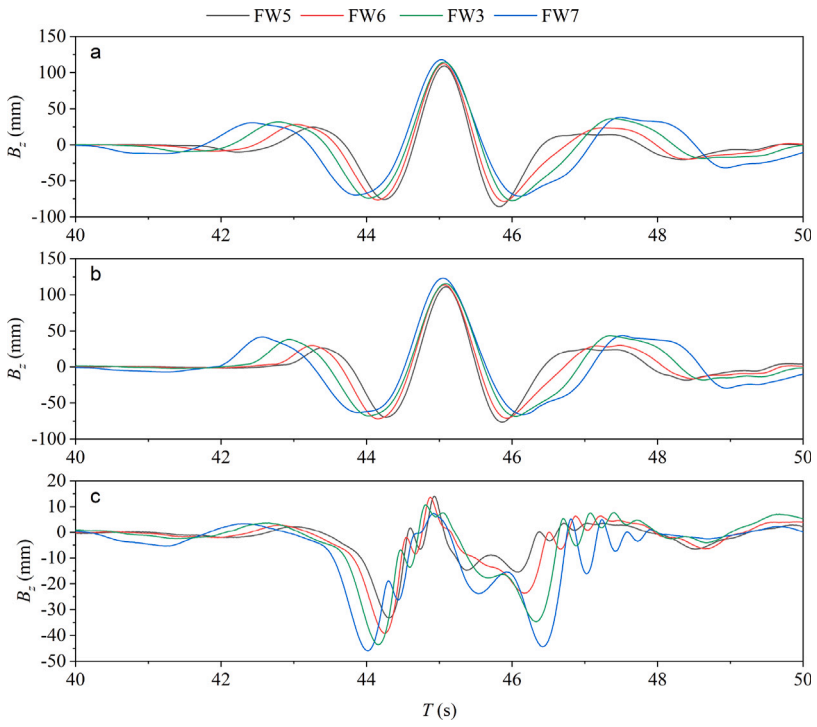

Fig. 17. Time history of the heave motion for different case FW5, FW6, FW3, and FW7 with various damping values d_0 (a), d_1 (b), and d_∞ (c).

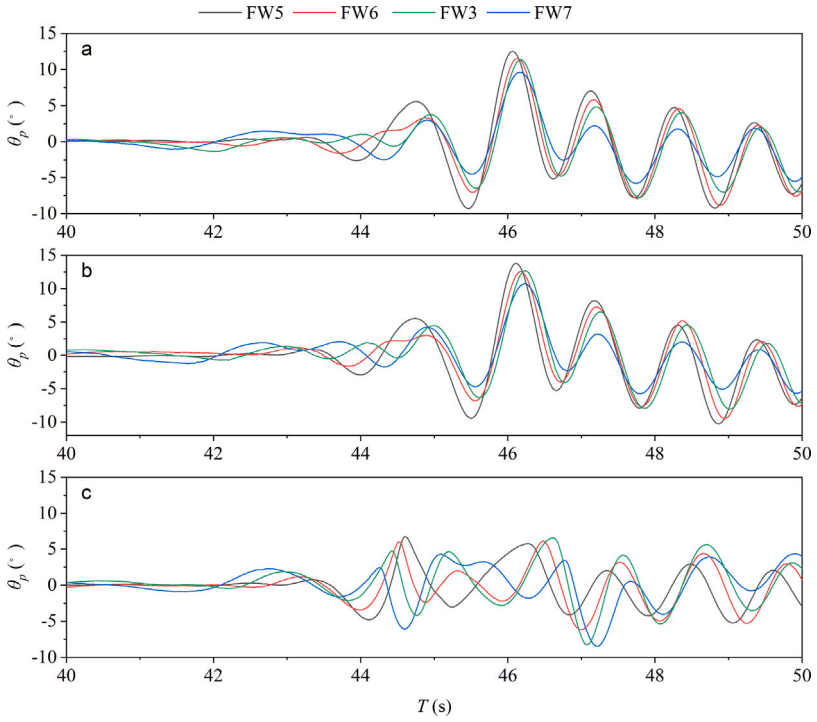

Fig. 18. Time history of the pitch motion for different case FW5, FW6, FW3, and FW7 with various damping values d_0 (a), d_1 (b), and d_∞ (c).

spring compression while this can be avoided by slightly increasing the PTO damping. Thus, the range of motion of the PTO translator for zero damping condition can be adjusted according to sea conditions to avoid large mooring forces caused by the taut mooring rope. It should be noted that the experimental model used in this study is limited to the laboratory scale. Lower end-stop systems and adjustable damping cases are not considered in this work. Therefore, these results should only be used as a reference for the initial design phase.

The findings of this experiment can be extended to other point-absorber wave energy converters that share similar system features and characteristics. The experiment utilized a constant PTO damping, and so with the implementation of a survivability control, the mooring line

may experience reduced force. Additionally, it is worth noting that there is no lower end-stop spring in this setup, and when analysing the overtopping phenomenon, the impact of this constraint should be considered, making it a point of interest for future studies. Many point-absorption WEC installations utilize a stroked PTO system (i.e., the presence of an end-stop system), including: Hydraulic PTO systems and Direct-drive PTO systems (Guo et al., 2022). Generally, there is a finite stroke length for movement of the float-driven PTO system.

CRediT authorship contribution statement

Guixun Zhu: Formal analysis, Investigation, Data curation, Writing – original draft, Writing – review & editing. **Zahra Shahroozi:** Conceptualization, Methodology, Writing – review & editing. **Siming Zheng:** Investigation, Supervision, Writing – review & editing. **Malin Göteman:** Supervision, Writing – review & editing. **Jens Engström:** Supervision, Writing – review & editing. **Deborah Greaves:** Supervision, Writing – review & editing.

Declaration of competing interest

The authors declare that they have no known competing financial interests or personal relationships that could have appeared to influence the work reported in this paper.

Data availability

Data will be made available on request.

Acknowledgements

The research was supported by the financial support from China Scholarship Council (Grant No. 201806060137). The authors would also like to acknowledge Dr K. Monk and Dr M. Hann for providing help in the ocean wave basin at Plymouth University.

References

Al Shami, E., Zhang, R., Wang, X., 2018. Point absorber wave energy harvesters: A review of recent developments. Energies 12 (1), 47.
Bai, W., Taylor, R.E., 2007. Numerical simulation of fully nonlinear regular and focused wave diffraction around a vertical cylinder using domain decomposition. Appl. Ocean Res. 29 (1–2), 55–71.
Bihs, H., Chella, M.A., Kamath, A., Arntsen, Ø.A., 2017. Numerical investigation of focused waves and their interaction with a vertical cylinder using REEF3D. J. Offshore Mech. Arct. Eng. 139 (4).
Borthwick, A.G., Hunt, A.C., Feng, T., Taylor, P.H., Stansby, P.K., 2006. Flow kinematics of focused wave groups on a plane beach in the UK coastal research facility. Coast. Eng. 53 (12), 1033–1044.
Brito, M., Canelas, R., García-Feal, O., Domínguez, J., Crespo, A., Ferreira, R., Neves, M., Teixeira, L., 2020a. A numerical tool for modelling oscillating wave surge converter with nonlinear mechanical constraints. Renew. Energy 146, 2024–2043.
Brito, M., Ferreira, R.M., Teixeira, L., Neves, M.G., Canelas, R.B., 2020b. Experimental investigation on the power capture of an oscillating wave surge converter in unidirectional waves. Renew. Energy 151, 975–992.
Brown, S.A., Ransley, E.J., Musiedlak, P.-H., Greaves, D., 2020. Quantifying the predictive capability of OpenFOAM 5.0: Focused wave impacts with floating bodies. Int. J. Offshore Polar Eng. 30 (01), 20–27.
Budal, K., Falnes, J., 1975. A resonant point absorber of ocean-wave power. Nature 256, 478–479.
Cassidy, M., Taylor, R.E., Houlsby, G., 2001. Analysis of jack-up units using a constrained NewWave methodology. Appl. Ocean Res. 23 (4), 221–234.
Chakrabarti, S.K., 1987. Hydrodynamics of Offshore Structures. WIT Press.
Chen, D., Feng, X., Hou, C., Chen, J.F., 2022a. A coupled frequency and time domain approach for hydroelastic analysis of very large floating structures under focused wave groups. Ocean Eng. 255, 111393.
Chen, H., Qian, L., Cao, D., 2023. Harmonic structure of the nonlinear force on a fixed ship-shaped floating production, storage and offloading vessel under dispersive phase-focused wave groups. Phys. Fluids 35 (4), 042103.
Chen, S., Zhao, W., Wan, D., 2022b. On the scattering of focused wave by a finite surface-piercing circular cylinder: A numerical investigation. Phys. Fluids 34 (3), 035132.
Clauss, G.F., 2010. Freak waves and their interaction with ships and offshore structures. In: Advances in Numerical Simulation of Nonlinear Water Waves. World Scientific, pp. 641–687.
Contestabile, P., Crispino, G., Di Lauro, E., Ferrante, V., Gisonni, C., Vicinanza, D., 2020. Overtopping breakwater for wave energy conversion: Review of state of art, recent advancements and what lies ahead. Renew. Energy 147, 705–718.
Cretel, J.A., Lightbody, G., Thomas, G.P., Lewis, A.W., 2011. Maximisation of energy capture by a wave-energy point absorber using model predictive control. IFAC Proc. Vol. 44 (1), 3714–3721.
Drew, B., Plummer, A.R., Sahinkaya, M.N., 2009. A review of wave energy converter technology. Proc. Inst. Mech. Eng., Part A: J. Power Energy 223 (8), 887–902.
Faizal, M., Ahmed, M.R., Lee, Y.H., 2014. A design outline for floating point absorber wave energy converters. Adv. Mech. Eng. 6, 846097.
Falcão, A.F.d.O., Henriques, J.C.C., 2016. Oscillating water column wave energy converters and air turbines: A review. Renew. Energy 85, 1391–1424.
Garcia-Teruel, A., Forehand, D.I., 2022. Manufacturability considerations in design optimisation of wave energy converters. Renew. Energy 187, 857–873.
Giannini, G., Rosa-Santos, P., Ramos, V., Taveira-Pinto, F., 2022. Wave energy converters design combining hydrodynamic performance and structural assessment. Energy 249, 123641.
Goda, Y., 2010. Reanalysis of regular and random breaking wave statistics. Coast. Eng. J. 52 (1), 71–106.
Göteman, M., Engström, J., Eriksson, M., Hann, M., Ransley, E., Greaves, D., Leijon, M., 2015. Wave loads on a point-absorbing wave energy device in extreme waves. In: The Twenty-Fifth International Ocean and Polar Engineering Conference. OnePetro.
Guo, B., Wang, T., Jin, S., Duan, S., Yang, K., Zhao, Y., 2022. A review of point absorber wave energy converters. J. Mar. Sci. Eng. 10 (10), 1534.
Hann, M., Greaves, D., Raby, A., 2015. Snatch loading of a single taut moored floating wave energy converter due to focussed wave groups. Ocean Eng. 96, 258–271.
Hann, M., Greaves, D., Raby, A., Howey, B., 2018. Use of constrained focused waves to measure extreme loading of a taut moored floating wave energy converter. Ocean Eng. 148, 33–42.
Hunt-Raby, A.C., Borthwick, A.G., Stansby, P.K., Taylor, P.H., 2011. Experimental measurement of focused wave group and solitary wave overtopping. J. Hydraul. Res. 49 (4), 450–464.
Jin, S., Greaves, D., 2021. Wave energy in the UK: Status review and future perspectives. Renew. Sustain. Energy Rev. 143, 110932.
Jin, S., Patton, R.J., Guo, B., 2018. Viscosity effect on a point absorber wave energy converter hydrodynamics validated by simulation and experiment. Renew. Energy 129, 500–512.
Jonathan, P., Taylor, P.H., 1997. On irregular, nonlinear waves in a spread sea. J. Offshore Mech. Arct. Eng. 119 (1), 37–41.
Judge, F.M., Hunt-Raby, A.C., Orszaghova, J., Taylor, P.H., Borthwick, A.G., 2019. Multi-directional focused wave group interactions with a plane beach. Coast. Eng. 152, 103531.
Katsidoniotaki, E., Nilsson, E., Rutgersson, A., Engström, J., Göteman, M., 2021. Response of point-absorbing wave energy conversion system in 50-years return period extreme focused waves. J. Mar. Sci. Eng. 9 (3), 345.
Lehmann, M., Karimpour, F., Goudey, C.A., Jacobson, P.T., Alam, M.-R., 2017. Ocean wave energy in the United States: Current status and future perspectives. Renew. Sustain. Energy Rev. 74, 1300–1313.
Li, A., Liu, Y., 2022. Hydrodynamic performance and energy absorption of multiple spherical absorbers along a straight coast. Phys. Fluids 34 (11), 117102.
Lindgren, G., 1970. Some properties of a normal process near a local maximum. Ann. Math. Stat. 41 (6), 1870–1883.
Margheritini, L., Vicinanza, D., Frigaard, P., 2009. SSG wave energy converter: Design, reliability and hydraulic performance of an innovative overtopping device. Renew. Energy 34 (5), 1371–1380.
Ning, D., Ding, B., 2022. Modelling and Optimization of Wave Energy Converters. CRC Press.
Ning, D., Wang, R.q., Chen, L.f., Sun, K., 2019. Experimental investigation of a land-based dual-chamber OWC wave energy converter. Renew. Sustain. Energy Rev. 105, 48–60.
Ning, D., Zang, J., Liu, S., Eatock Taylor, R., Teng, B., Taylor, P., 2009. Free-surface evolution and wave kinematics for nonlinear uni-directional focused wave groups. Ocean Eng. 36 (15–16), 1226–1243.
Rafiee, A., Fiévez, J., 2015. Numerical prediction of extreme loads on the CETO wave energy converter. In: Proceedings of the 11th European Wave and Tidal Energy Conference, Nantes, France. (09A1-2).
Ransley, E.J., Brown, S.A., Hann, M., Greaves, D.M., Windt, C., Ringwood, J., Davidson, J., Schmitt, P., Yan, S., Wang, J.X., et al., 2021. Focused wave interactions with floating structures: A blind comparative study. Proceedings of the Institution of Civil Engineers-Engineering and Computational Mechanics 174 (1), 46–61.
Ransley, E., Greaves, D., Raby, A., Simmonds, D., Hann, M., 2017. Survivability of wave energy converters using CFD. Renew. Energy 109, 235–247.
Ransley, E., Yan, S., Brown, S., Hann, M., Graham, D., Windt, C., Schmitt, P., Davidson, J., Ringwood, J., Musiedlak, P.-H., et al., 2020. A blind comparative study of focused wave interactions with floating structures (CCP-WSI Blind Test Series 3). International Journal of Offshore and Polar Engineering 30 (01), 1–10.

Shahroozi, Z., Göteman, M., Engström, J., 2022. Experimental investigation of a point-absorber wave energy converter response in different wave-type representations of extreme sea states. Ocean Eng. 248, 110693.

Soleimani, K., Ketabdari, M.J., Gharechae, A., 2023. Smoothed particle hydrodynamics study of a heaving point absorber in various waves using wave tank and calm-water models. Phys. Fluids 35 (3), 033116.

Taylor, P., Williams, B., 2004. Wave statistics for intermediate depth water—NewWaves and symmetry. J. Offshore Mech. Arct. Eng. 126 (1), 54–59.

Tromans, P.S., Anaturk, A.R., Hagemeijer, P., 1991. A new model for the kinematics of large ocean waves-application as a design wave. In: The First International Offshore and Polar Engineering Conference. OnePetro.

Walker, D.A., Taylor, R.E., 2005. Wave diffraction from linear arrays of cylinders. Ocean Eng. 32 (17–18), 2053–2078.

Westphalen, J., Greaves, D., Williams, C., Hunt-Raby, A., Zang, J., 2012. Focused waves and wave–structure interaction in a numerical wave tank. Ocean Eng. 45, 9–21.

Westphalen, J., Greaves, D., Williams, C., Taylor, P., Causon, D., Mingham, C., Hu, Z., Stansby, P., Rogers, B., Omidvar, P., 2009. Extreme wave loading on offshore wave energy devices using CFD: A hierarchical team approach. In: Proceedings of the 8th European Wave and Tidal Energy Conference. pp. 500–508.

Whittaker, C., Fitzgerald, C., Raby, A.C., Taylor, P., Orszaghova, J., Borthwick, A., 2017. Optimisation of focused wave group runup on a plane beach. Coast. Eng. 121, 44–55.

Zang, J., Taylor, P.H., Morgan, G., Stringer, R., Orszaghova, J., Grice, J., Tello, M., 2010. Steep wave and breaking wave impact on offshore wind turbine foundations–ringing re-visited. In: 25th International Workshop on Water Waves and Floating Bodies. pp. 9–12.

Zhang, Y., Zhao, Y., Sun, W., Li, J., 2021. Ocean wave energy converters: Technical principle, device realization, and performance evaluation. Renew. Sustain. Energy Rev. 141, 110764.

Zhao, X., Ye, Z., Fu, Y., Cao, F., 2014. A CIP-based numerical simulation of freak wave impact on a floating body. Ocean Eng. 87, 50–63.

Zheng, S., Antonini, A., Zhang, Y., Greaves, D., Miles, J., Iglesias, G., 2019. Wave power extraction from multiple oscillating water columns along a straight coast. J. Fluid Mech. 878, 445–480.

Zhu, G., Samuel, J., Zheng, S., Hughes, J., Simmonds, D., Greaves, D., 2023. Numerical investigation on the hydrodynamic performance of a 2D U-shaped oscillating water column wave energy converter. Energy 274, 127357.